Directed Energy Transfer in Films of CdSe Quantum Dots: Beyond the Point Dipole Approximation

8 AUTHORS, INCLUDING:

Kaibo Zheng
Lund University
47 PUBLICATIONS   **663** CITATIONS

SEE PROFILE

Mohamed Abdellah
Lund University
28 PUBLICATIONS   **366** CITATIONS

SEE PROFILE

Qijin Chi
Technical University of Denmark
98 PUBLICATIONS   **2,298** CITATIONS

SEE PROFILE

Tönu Pullerits
Lund University
179 PUBLICATIONS   **5,418** CITATIONS

SEE PROFILE

Directed Energy Transfer in Films of CdSe Quantum Dots: Beyond the Point Dipole Approximation

Kaibo Zheng,[†] Karel Žídek,[†] Mohamed Abdellah,[†,‡] Nan Zhu,[§] Pavel Chábera,[†] Nils Lenngren,[†] Qijin Chi,[§] and Tõnu Pullerits*,[†]

[†]Department of Chemical Physics, Lund University, Box 124, 22100, Lund, Sweden
[§]Department of Chemistry, Technical University of Denmark, DK-2800 Kongens Lyngby, Denmark
[‡]Department of Chemistry, Faculty of Science, South Valley University, Qena 83523, Egypt

S *Supporting Information*

ABSTRACT: Understanding of Förster resonance energy transfer (FRET) in thin films composed of quantum dots (QDs) is of fundamental and technological significance in optimal design of QD based optoelectronic devices. The separation between QDs in the densely packed films is usually smaller than the size of QDs, so that the simple point—dipole approximation, widely used in the conventional approach, can no longer offer quantitative description of the FRET dynamics in such systems. Here, we report the investigations of the FRET dynamics in densely packed films composed of multisized CdSe QDs using ultrafast transient absorption spectroscopy and theoretical modeling. Pairwise interdot transfer time was determined in the range of 1.5 to 2 ns by spectral analyses which enable separation of the FRET contribution from intrinsic exciton decay. A rational model is suggested by taking into account the distribution of the electronic transition densities in the dots and using the film morphology revealed by AFM images. The FRET dynamics predicted by the model are in good quantitative agreement with experimental observations without adjustable parameters. Finally, we use our theoretical model to calculate dynamics of directed energy transfer in ordered multilayer QD films, which we also observe experimentally. The Monte Carlo simulations reveal that three ideal QD monolayers can provide exciton funneling efficiency above 80% from the most distant layer. Thereby, utilization of directed energy transfer can significantly improve light harvesting efficiency of QD devices.
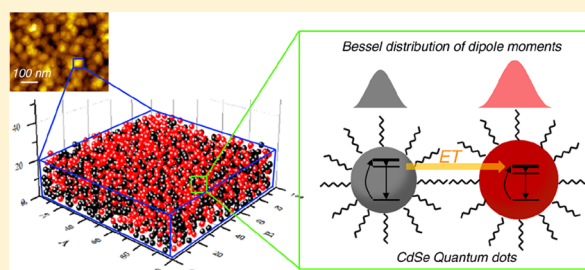
INTRODUCTION

Semiconductor quantum dots (QDs) hold promises for a broad spectrum of applications. For example, QDs are novel light harvesters for next generation solar cells due to their high extinction coefficient, ability to generate multiple excitons, size-dependent tunability of bandgap, and high stability.[1−8] They are also efficient light emitters, and therefore can be used in fabrication of light-emitting diodes and QD lasers.[9−11] In the development of such devices, QDs are often densely packed to form a thin film with strong absorption or emission. Förster resonant energy transfer (FRET) induced by electronic coupling between QDs is an essential process for function of such devices.[12] Since the process has a significant impact on optoelectronic properties of QD layers, detailed understanding of FRET, its dynamic features in particular, is of both fundamental and technological importance. For instance, in conventional Grätzel-type QD sensitized solar cells, electron injection occurs from directly attached QDs to acceptors. Although this process can be fast (∼ps), the overall efficiency of the solar cells is likely limited by insufficient utilization of the sun light with monolayer QDs coverage.[13] The problem can be solved by using band gap-controlled multilayered QDs where energy is funneled toward electrodes via FRET.[14−16]

FRET is a vital process in photosynthetic light harvesting[17] and has been widely used to describe excitation dynamics in conjugated polymers as well.[18] Time-resolved fluorescence studies of the films of QDs with different sizes have provided clear evidence for FRET from smaller to larger size QDs.[15] Time-constant of such transfer depends strongly on the system and has been reported to be from about a nanosecond down to few tens of picoseconds.[16,19−25]

It is generally accepted that the usual point dipole approximation in FRET is valid if the excitation donor and acceptor separation is significantly larger than the size of them. In cases of closely lying molecular donor—acceptor systems, various refinements to the approximation have been suggested, like atom-centered transition monopoles,[26,27] continuous transition densities,[28] or partial dipoles.[29] Already, early studies of FRET in QD films pointed out that higher multipole interactions should probably be considered for the excitation transfer between closely packed QDs.[30] However, to the best of our knowledge no such attempts have been reported so far.
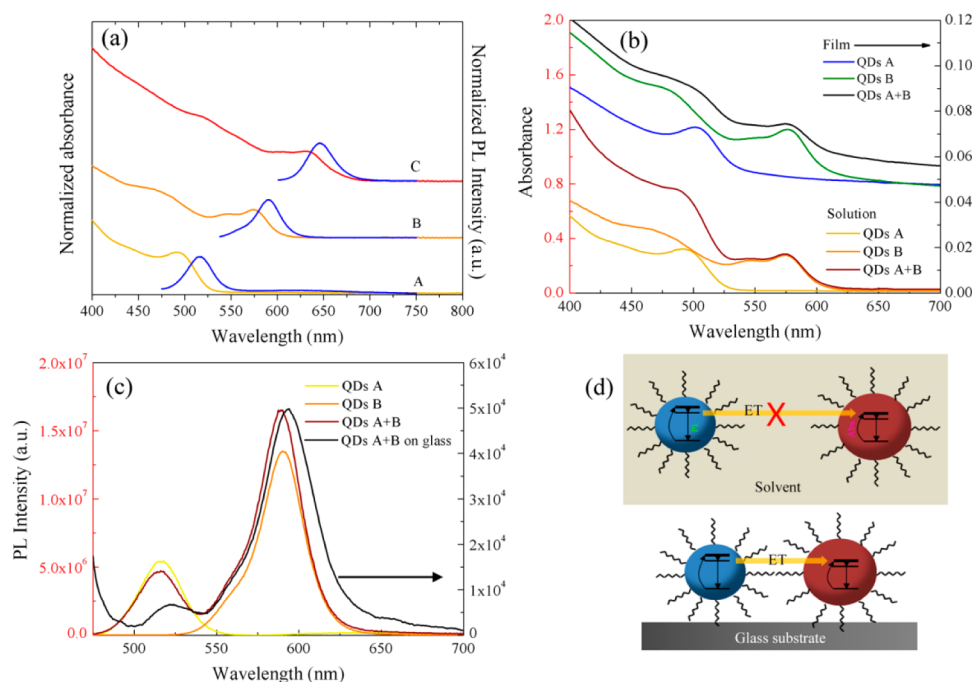
Figure 1. Steady-state spectroscopy. (a) Absorption and photoluminescence (blue lines) spectra of CdSe QDs with three different mean sizes (A: 2.3 nm; B: 3.7 nm; C: 6.6 nm). (b) Absorption spectra and (c) photoluminescence (λ_{exc} = 470 nm) of colloidal CdSe QDs A (yellow), B (orange), QDs A+B (wine) (1:1 molar ratio), and QDs A (blue), QDs B (green), QDs A+B (purple) deposited onto glass (black). The left axis corresponds to the colloidal solution and the right axis to the film samples. (d) Schematic illustration of FRET within a two-sized QD system in solution form and thin film form.

Here we calculate FRET between QDs by taking into account the distribution of the dipole moment over the volume of QD. We show that the approach gives an important correction to the FRET if the QDs are closer than approximately three QD diameters—the usual case in densely packed QD films. To compare the refined theory and experiments, we use transient absorption (TA) measurements and apply time-dependent species associated spectral analyses which enables disentanglement of intrinsic exciton recombination from FRET. The experimental work is supplemented by Monte Carlo simulations of mixed QD films resembling the studied random samples. We use the calculations to determine the FRET rate distribution and dynamics with a very good agreement between theory and experiment.

Finally, to demonstrate implications of our findings on the energy transfer in QD systems, we experimentally and theoretically study directed FRET in ordered QD layers and show that QD layers, which are sequentially deposited, can yield exciton collection efficiency above 80%. The theoretical results are in good agreement with our experimental observations in the ordered multilayer QD films.

■ EXPERIMENTAL SECTION

Preparation and Characterization of Samples. Oleic acid-capped CdSe QDs were synthesized using previously reported methods.[31] Size of the QDs was tuned by controlling the reaction temperature. In this work, reaction temperatures 220, 280, and 320 °C were used to obtain QDs with the diameter of 2.3, 3.7, and 6.7 nm, respectively. All the as-synthesized QDs were able to be dispersed stably in toluene with the concentration of 10 mM as stock solution.

Multisized QD films were prepared by two methods. In the first method, two sizes of QDs were mixed at 1:1 volume ratio, and then spin-coated onto a glass substrate at a spinning rate of 1000 rpm for 30 s. Afterward 10% 3-mercaptopropionic acid (MPA) in methanol was spin-coated at the same conditions to exchange the oleic acid

capping agent of the as-obtained QDs. Then the film was rinsed using methanol and toluene to remove excessive QDs and MPA. This deposition process is repeated several times to form a thick layer of QDs. All results presented here were measured on samples prepared by this method.

In the second method, the capping agent of QDs was directly exchanged after synthesis by MPA using a previously reported method and redispersed in ethanol.[31] A mixture of two sizes of MPA-capped QDs in solution (1:1 volume ratio) was then spin-coated onto glass substrate at 1000 rpm for 30 s without further treatment. The second method was used to verify that original QD capping (oleic acid) does not affect the QD−QD distance in the resulting film, thus affecting the FRET rate (Supporting Information).

The morphology of multisized QD assemblies was imaged in the tapping mode by atomic force microscopy (AFM) (AFM 5500 System, Agilent Technologies) and a scanning electron microscope (SEM) (SU8010, HITACHI, resolution 1 nm) with accelerating voltage of 10 kV and working distance of 3.5 mm.

Steady-State Spectroscopy. Ground-state absorption spectra were measured in a UV−vis absorption spectrometer (Agilent 845x). Steady-state photoluminescence (PL) of the QD films and colloidal solutions was measured using a standard spectrophotometer (Spex 1681) with excitation at 470 nm (steady-state characterization) and 420 nm (ordered multilayer film study) under N_2 atmosphere.

Transient Absorption Kinetics. Transient absorption kinetics was recorded using a standard pump−probe setup as in our previous study.[31] Laser pulses (800 nm, 80 fs pulse length, 1 kHz repetition rate) were generated by a regenerative amplifier (Spitfire XP) seeded by a femtosecond oscillator (Tsunami, both Spectra Physics). Excitation pulses at the wavelength of 430 nm were acquired using an optical parametric amplifier (Topas C, Light Conversion). The excitation photon flux used of 2×10^{14} photons/cm²/pulse corresponds to $\langle N \rangle \sim 0.2-0.35$ (the mean number of excited e−h pairs per QD), depending on the QD size. The probe pulses (broad supercontinuum spectrum) were generated from the 800 nm pulses in a sapphire plate and split by a beam splitter into probe pulse and a reference pulse. The probe pulse and the reference pulse were
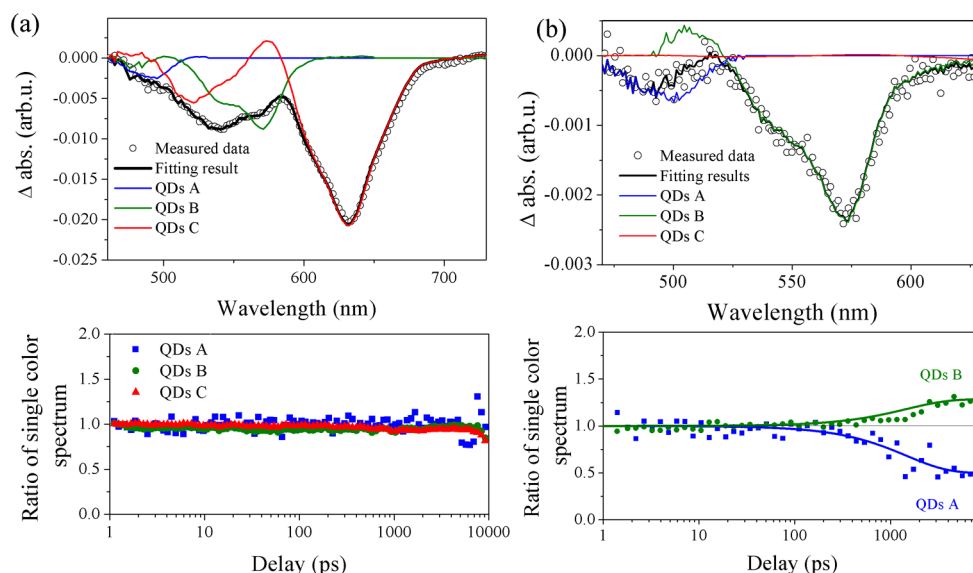
Figure 2. Comparison of TA spectra and fittings for mixed QDs in the solution and solid thin film forms. (a) TA spectra of single-sized QDs A (blue line), B (green line), C (red line), and mixed QDs A+B+C (open circles) in colloidal form at a time delay of 1 ns. The black line refers to the optimal fitting of mixed QDs A+B+C solution by a sum of single-color spectra (A ~ C) for the same delay. (b) TA spectra of single-sized QDs A, B, and C and mixed QDs A+B (open circles) deposited on glass at a time delay of 1 ns. The black line refers to the optimal fitting by the same method. Lower panels of (a) and (b) show the dependence of contribution of each color on pump−probe delay corresponding to (A+B+C) solution and (A+B) film, respectively.

dispersed in a spectrograph and detected by a diode array (Pascher Instruments). Colloidal samples with typical optical density (OD) of 0.2 at first exciton peak were measured in a static cell (1 mm pathway). Thin film samples (typical OD of 0.02 at first exciton peak) were measured in a nitrogen atmosphere to avoid possible oxidation of QDs.[32]

■ RESULTS AND DISCUSSION

Steady-State Spectroscopy. Three sizes of CdSe QDs were employed in our study. Figure 1a shows the UV−vis absorption and photoluminescence spectra of each size of QDs in a colloidal form. The absorption spectra of all samples exhibit clear band-like exciton peak due to strong quantum confinement.[26] The mean size of each QD can be estimated by the position of the band-edge absorption peaks (493, 575, and 635 nm) to be 2.3 nm (defined as QDs A), 3.7 nm (defined as QDs B), and 6.6 nm (defined as QDs C), respectively.[33] The narrow width (~25 nm) in all emission spectra (blue lines in Figure 1a) indicates that the synthesized QDs are uniform with only a small size variation. In addition, except for a weak red-shifted photoluminescence detected in the QD A, almost no defect-related band is observed, indicating good surface passivation and a very limited amount of defects in the QDs.

We prepared colloidal solutions and thin films of the QDs where two different sizes of the dots are used. Samples with three different two-size combinations (i.e., A+B, A+C, B+C) were obtained. The absorption spectrum of the mixture of the QDs corresponds well to the sum of the corresponding pure QD spectra both as a solution and as a film (e.g., Figure 1b for the mixture of QDs A+B).

The emission spectrum of the mixture in solution is nearly the same as the sum of the emissions of the two samples with different sizes. At the same time the emission of the mixture film shows a typical indication of FRET (see Figure 1c): energy transfer from smaller to larger QDs manifests itself as a significant reduction of the blue emission accompanied by an increase of the red emission. The ratio between red and blue

emission for thin film samples (7.4) is much higher than that for mixed solution form (3.5) or in the case of separately measured single-sized colloidal QDs (2.5). Note that the difference between the ratios in mixed solution form (3.5) and separated solutions (2.5) can be fully explained by reabsorption of emitted photoluminescence on the blue side, not FRET (Supporting Information). This effect is observable in solution due to a rather high OD (0.2 at first exciton peak). The effect is negligible in thin film samples with a significantly lower OD (~0.02 at first exciton peak).

Hence, the steady-state spectroscopy has led to a conclusion that FRET between QDs likely occurs in the thin film samples as illustrated in Figure 1d. However, the steady-state spectra do not provide a full proof of FRET—changes in emission can partly originate from trap states formed during deposition of QD films. Second, steady-state spectroscopy cannot reveal time scales of the FRET processes. Therefore, our analysis of the energy transfer will rely on transient absorption measurements as described below.

Transient Absorption Spectroscopy. The FRET dynamics in multisized QD mixtures were investigated by TA spectroscopy. The TA spectra of single-sized QDs show strong bleach at the band-edge absorption region (Supporting Information). This is caused by the state filling of 1S electron states of the conduction band after photoexcitation. The recovery of the bleach takes place on a nanosecond time scale (mean lifetimes of 24−28 ns; see Supporting Information), in line with our previous results.[15,31,34]

In two-sized QD systems the excitation does not have selectivity therefore the initial bleach of the band edge exciton transition occurs in both QDs. In many previous studies, analysis has been based on comparing differences between the mean excited state lifetimes in single-sized and mixed films providing information about FRET. Here we perform time dependent species associated spectral analyses.[35] First we measure TA spectra for different delays *t* for each size of QD

separately ($\Delta\alpha_A(t)$, $\Delta\alpha_B(t)$, $\Delta\alpha_C(t)$) and then for two-size mixtures (A+B, A+C, B+C). In the following we explain the procedure using the TA spectrum of A+B mixture, $\Delta\alpha_{A+B}(t)$, as an example. All other mixtures are analyzed in the same way.

For all measured delays t we fit the TA spectrum of mixture $\Delta\alpha_{A+B}(t)$ as a sum of TA spectra of each size of QD at the same delay ($\Delta\alpha_A(t)$ and $\Delta\alpha_B(t)$):

$$\Delta\alpha_{A+B}(t) = k_A(t)\Delta\alpha_A(t) + k_B(t)\Delta\alpha_B(t) \qquad (1)$$

It is worth stressing that in the analysis the mixtures of QDs in solutions were always fitted by single-sized QD solutions and, analogously, the mixed films were only fitted by the single-sized QD films. The single-sized spectra were cropped in regions, where the respective QDs do not display any signal. By doing this we reduced the noise of fitted coefficients $k_{A,B}(t)$.

We can rescale the fitting coefficients $k_{A,B}(t)$ from eq 1 according to their value close to the zero delay $k_{A,B}(0)$. The ratio $k_{A,B}(t)/k_{A,B}(0)$, which we will hereafter call as "ratio of the single-color spectrum" gives us important information about FRET dynamics. If there is no FRET present in the system, the ratios will stay constant, because the time evolution of $\Delta\alpha_A(t)$ and $\Delta\alpha_B(t)$ already includes the intrinsic decay of excitons in QDs due to fluorescence, surface trapping, photocharging, or a rapid Auger recombination.[36,37] We will later demonstrate it for a diluted colloidal sample. The time dependences of the $k_{A,B}(t)/k_{A,B}(0)$ ratio corresponds to the FRET-related change of the excited state population in A and B relative to their initial excitation. We even obtain quantitative scale of FRET as we can compare decrease of TA signal, i.e., population, of donor QDs (here A) compared to their initial population. Note that the corresponding increase in the acceptor part (here B) can have different amplitude, as it is normalized to the initial population of acceptors.

As we have mentioned already, for a mixture of non-interacting QDs, we should observe a constant ratio $k_{A,B}(t)/k_{A,B}(0)$ for all delays. To verify this expectation, we have recorded the TA spectra of each single-size QDs and a mixture of QDs (A+B+C) in diluted solutions. Figure 2a illustrates the methodology used in the fittings. For one chosen delay (1 ns in this case), we fit the total TA spectrum (open circles) as a sum of single-color spectra (blue, green, and red line). We can see that the total fit (black line) reproduces the measured data very well. Apparently, the ratio of excited colors also stays constant over the whole time range—in this case from 1 ps up to 10 ns, i.e., 4 orders of magnitude. This is clear proof that there is no exciton migration in this mixture.

On the contrary, after deposition as solid film, the same procedure with a two-size mixture of QDs shows significant changes of single size ratios (see Figure 2b). This is illustrated by an example of QDs A+B in a thin-film form. The spectrum ratio of QDs A (2.3 nm) decreases, accompanied by an increase of spectrum ratio of QDs B (3.7 nm). Both kinetics are very similar. In addition to the previously presented steady-state spectroscopy measurements, these measurements and analysis add quantitative information about the FRET dynamics from small QDs to larger QDs.

In order to compare our results with the previously published transfer rates in the literature, we have fitted both donor and acceptor k kinetics by a single exponential decay/growth, leading to the same lifetime of (1.5 ± 0.5) ns, which is an expected FRET time in a closely packed film of QDs. However, this single FRET lifetime, as we will show later, is only a very simple sketch of the true dynamics.

We analyzed the other two combinations of QDs (B+C, A+C) in the same fashion. The results shown in Figure 3 are
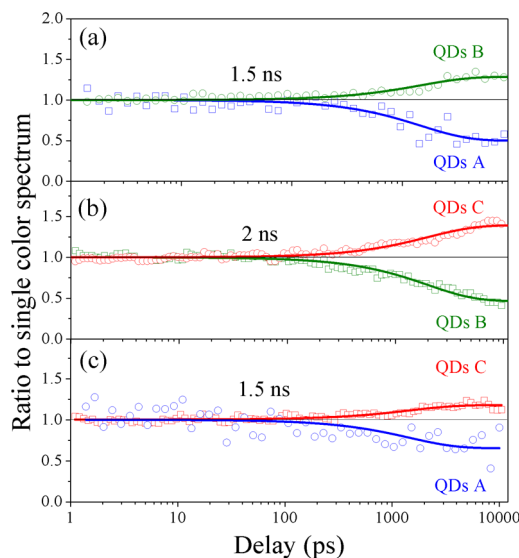
Figure 3. Dynamics of the contribution of each size of QDs to the total TA signal measured within two-size-mixed QDs deposited on glasses: (a) QDs A+B, (b) QDs B+C, and (c) QDs A+C. Open circles correspond to the ratios $k_{A,B}(t)/k_{A,B}(0)$ from the species associated spectral analyses, and solid lines are the exponential fits (see text for detail).

analogous and lead to a mean ET lifetime of (2.0 ± 0.8) ns and (1.5 ± 0.6) ns for (B+C) and (A+C) systems, respectively. Obviously, the trend of the ET time cannot be simply related to the center-to-center distances between the QDs where $D_{B\sim C} > D_{A\sim C} > D_{A\sim B}$, which itself should lead to approximately $1/r^6$ dependence of lifetimes on the distances. In the following part, we will present a rigorous model taking into account all the possible parameters in randomly arranged QD systems, which will rationalize the observed FRET rates. We will also show that describing the FRET in closely packed QD films by a simple model of ideally stacked QDs and point dipoles is insufficient.

Role of Dipole Distribution in FRET between QDs. The standard FRET theory calculates energy transport rate between two point dipoles as[12]

$$k_{ET} = 1/\tau_{ET} = R_{DA}^6 n^4 / \left(\frac{2\pi}{\hbar} \mu_D^2 \mu_A^2 K^2 \theta \right) \qquad (2)$$

where μ_A and μ_D are the donor and acceptor transition dipoles, R_{DA} is the distance between donor and acceptor, Θ is the spectral overlap integral between normalized donor emission and acceptor absorption line shapes, κ^2 refers to the orientation factor of the dipole–dipole interaction, and n is the medium's refractive index. This is a valid approach for two QDs (or any systems) separated by a distance much larger than their own dimensions. However, in densely packed QD film the distance between QDs can be very small and, as we will show in the following paragraphs, the precondition of the point–dipole approximation is not satisfied.

Wave functions of electrons and holes in a QD are distributed over the whole QD volume. The infinite-barrier model of spherical QD implies that radial dependence of the wave function of an exciton in a QD features the Bessel function shape. For the lowest excited state of a QD with radius R, we can use[38]
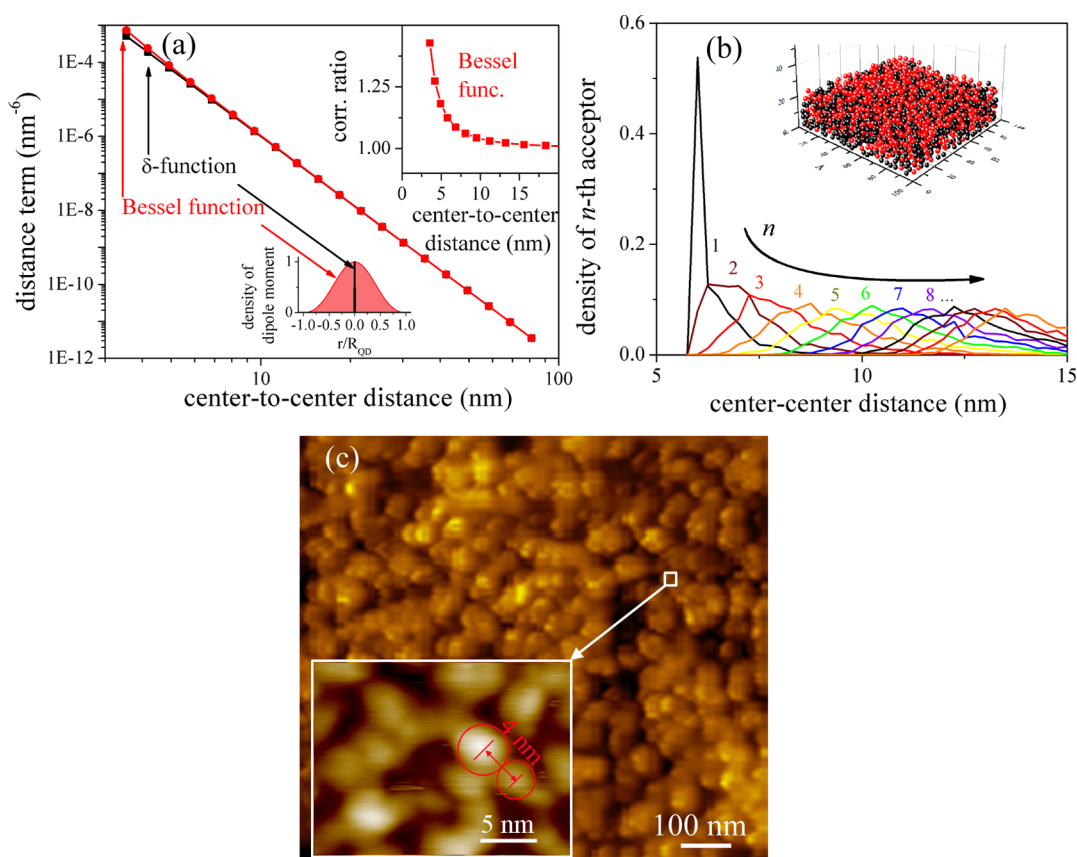
Figure 4. Simulation and AFM characterization of realistic QD thin films. (a) Distance term of FRET for δ-function approximation ($1/r^6$, black points) and Bessel function model (red points)—see inset in the middle for the corresponding density of dipole moments in the models. Upper inset: ratio between distance terms obtained via Bessel function and δ-function models. (b) Simulated deposition of two sizes of QDs into a random layer. The deposition leads to a distribution in the donor−acceptor distance. The distance to the 1st, 2nd, 3rd, ..., and nth acceptor is determined for 30 layers (100 QDs in the center of the layer). (c) AFM images of real mixed QDs (A+B) deposited on the silicon wafer, and the inset with larger magnification shows two neighboring QDs (A and B) with a center−center distance of 4 nm.

$$\rho(r) = \frac{1}{Norm} \frac{\sin\left(\frac{\pi r}{R}\right)}{\left(\frac{\pi r}{R}\right)} \tag{3}$$

Then dipole moment density $D(r)$ can be evaluated as $D(r) \propto \rho(r)$. $D(r)$ drops quickly with increasing distance from QD center (see Figure 4a, lower inset), but still the distribution can influence interaction of two close QDs.

In order to incorporate the dipole distribution into the FRET theory, we have modified the "$1/r^6$" term, which we will hereafter call "distance term". Namely, to evaluate FRET between two QDs with a center-to-center distance of r_{CC} we have carried out numerical integration of a dipole−dipole interaction (proportional to $1/r^3$) over the volume of the two QDs in spherical coordinates:

$$V(r_{CC}) = \int_{r_1,\varphi_1,\theta_1} \int_{r_2,\varphi_2,\theta_2} \frac{1}{(r_1 - r_2)^3} D(r_1, \varphi_1, \theta_1)$$
$$D(r_2, \varphi_2, \theta_2) \sin(\varphi_1) r_1^2 \sin(\varphi_2) r_2^2 \tag{4}$$

Each QD is divided into more than 20 segments along three spherical coordinates with the respective contribution weighted by a Jacobian. Division into 20 segments is sufficient for calculation convergence if r_{CC} is larger than 1.1 QD diameter. In other words, we divide each QD into 8000 point dipoles and calculated the dipole interaction term between each of them. In the end, the contribution from all segments is summed up and

$|V(r_{CC})|^2$ is calculated, since the transfer rate is proportional to the square of interaction in the Fermi's golden rule.

Figure 4a compares the distance term of FRET rate based on the numerical calculation of two approaches: one employs the dipole moment distributed as the Bessel function (red squares), and the second one uses the standard point dipole moment density (black squares). The calculation was done for FRET distance term between A-type QD (size of 2.3 nm) and B-type QD (size of 3.7 nm). As expected, for a large distance between QDs, the point−dipole approximation is sufficient and both calculations lead to the same results. However, for distances less than 10 nm, the point−dipole theory underestimates the resulting FRET rate. This is due to increased interaction between close parts of the QDs, where the distance is now significantly shorter compared to the center-to-center distance. For closely stacked QDs, the correction of the distance term on Bessel distribution can be more than 50%.

Role of Morphology in FRET between QDs. Another important aspect of FRET rate calculations in a closely packed film is realistic QD−QD distance determination. Commonly, a QD film is approximated by ideally stacked QD layers. Our AFM measurements (Figure 4c) show that in our case the films are quite far from this ideal model.

The morphology of the QD film is affected by its preparation. After spin coating onto the substrate, the capping agent OA was exchanged with MPA in order to immobilize the QDs for periodic deposition. Since OA (1.4 nm) is longer than

MPA (0.5 nm), after ligand exchange, QDs tend to aggregate into clusters to release the extra interdot space (Figure 4c) which is analogous to previously reported results.[39] The size of these clusters is around 50 nm, and within a cluster compact, individual QDs can still be identified by high-resolution AFM images. See, for example, the inset image in Figure 4c. In addition, the inset illustrates a typical case of closely attached A and B QDs showing that the center-to-center distance is about 4 nm. Considering that the radius of the two QDs is 1.15 and 1.85 nm gives the separation distance of 1 nm, which is exactly the length of two capping agent MPA molecules (Supporting Information).

We have simulated QD deposition in a way which mimics this real case. During the simulation, initially a random layer of QDs is placed at the bottom (zero level). Consequently new QDs are "deposited" on top of the first layer in random positions to fill all possible vacant places. The random deposition is repeated several times until a thick layer of QDs is obtained. An example of such a layer is depicted in Figure 4b. For each case we have prepared about 30 different random layers. As the next step, we pick 100 QDs inside the random layer which gives a similar dimension of the QD cluster as the real case (Figure 4c). For each QD in the cluster we determine the center-to-center distance to the closest QD, second closest QD, ..., and nth closest QD.

We point out that the layer is formed by two sizes of QDs (red and black dots in the inset of Figure 4b)—it is also done the same way in experimental preparation.

The analysis of a large population of QDs allows us to construct distribution histograms as shown in Figure 4b. From the histograms it is clear that the distance to the closest QD is relatively well-defined. In most cases it is the distance of QDs separated only by a linker layer. However, distance to other neighbors starts to have a big dispersion, increasing with n. This is a consequence of randomness of our cluster which is not present in ideal models.

An additional benefit of the direct simulation of the QD layers consists of obtaining a realistic volume fraction of QDs in the layer ($\sim$0.2 in all cases) as well as linker layers ($\sim$0.15). Here 65% of voids in the densely packed film might seem a surprisingly high value, but it should be noted that a ball fills only 52% of the corresponding cube. This means that from our model we still obtain a densely packed film. By using the Bruggeman model we can determine from the refractive index of CdSe (2.7), the linker layer ($\sim$1.4), and air (1), the effective refractive index of the whole layer (1.28 to 1.35) (Supporting Information).[39]

Calculation of FRET Rates. It is possible to perform the above-described simulation for all QD films studied experimentally in this work. For each case we get different histograms of the QD distance to the nth closest neighbor. From the histogram we can determine probability p(R_{cc1}, ..., R_{ccn}) of a QD having its first neighbor at distance R_{cc1}, ..., and nth neighbor at distance R_{ccn}. We can also determine the rate of Förster transfer for such combination of QD distances—it will be the sum of transfer rates to each of the neighbor:

$$k_{ET}(R_{cc1}, ..., R_{ccn}) = k_{ET}(R_{cc1}) + k_{ET}(R_{cc2}) + ...$$
$$+ k_{ET}(R_{ccn}) \qquad (5)$$

By using the FRET theory extended by Bessel function distribution of dipole moments (eq 4), we obtain k_{ET} rate for each combination and their sum. Because the position of the

nth neighbor is not a single value, but a distribution, we obtain distribution of FRET rates with various probabilities and we can create a histogram of the rates (see Figure 5). Parameters used to calculate the FRET rate for each case are listed in Table 1. Histograms of QD–QD distances for each case can be found in SI.
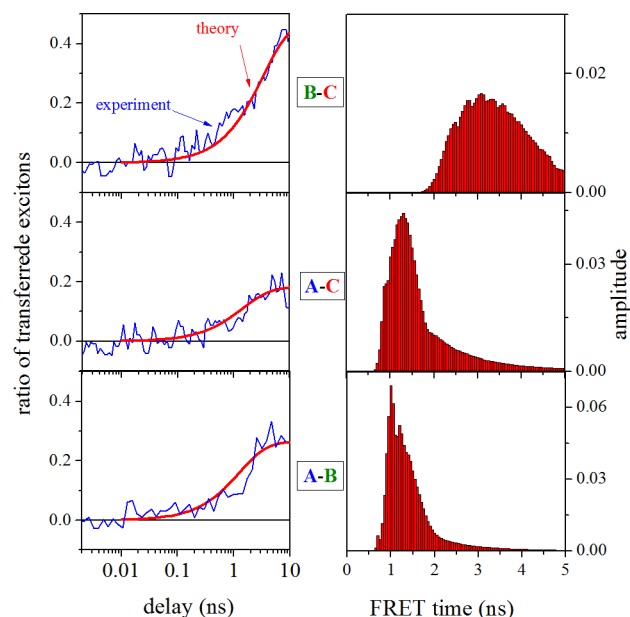

Figure 5. Ratio of transferred excitons and distribution of FRET lifetimes. Left panels: experimental ratio of the excitons transferred (0 ↔ no FRET, 1 ↔ all excitons transferred) to donor (blue lines) compared to the theoretical prediction (red line). Right panels: distribution of FRET lifetimes for each modeled case (see text for details).

Table 1. List of the Key Parameters Used in the Calculations of FRET Rates

key parameters	A+B	A+C	B+C
volume fraction of QDs (%)	16	24	24
volume fraction of linkers (%)	20	14	15
volume fraction of air (%)	64	62	61
refractive index of a QD		2.7	
refractive index of the linker		1.4	
refractive index of air		1	
effective refractive index	1.28	1.35	1.35
spectral overlap (10^{16} 1/mol 1/cm 1/nm)	1.17	10.9	12.2
donor quantum yield (%)	12	12	8
mean donor exciton lifetime (ps)	24 000	24 000	28 000
R_0 (nm)	5.6	7.8	7.4

Now we can turn to the obtained FRET rate distributions (see Figure 5). The FRET rate is mostly determined by the distance to the closest neighbor, and this distance is relatively well determined even in the random layer. Therefore, the rates form a distribution around a mean value on a nanosecond time scale (see Figure 5)—in all cases the mean value agrees (within experimental error) with the FRET rate determined by a simple single-exponential fitting of data.

When we reconstruct the expected curves of FRET (red lines) and compare them to our experimental results (blue lines), we obtain a remarkable agreement in all cases. We
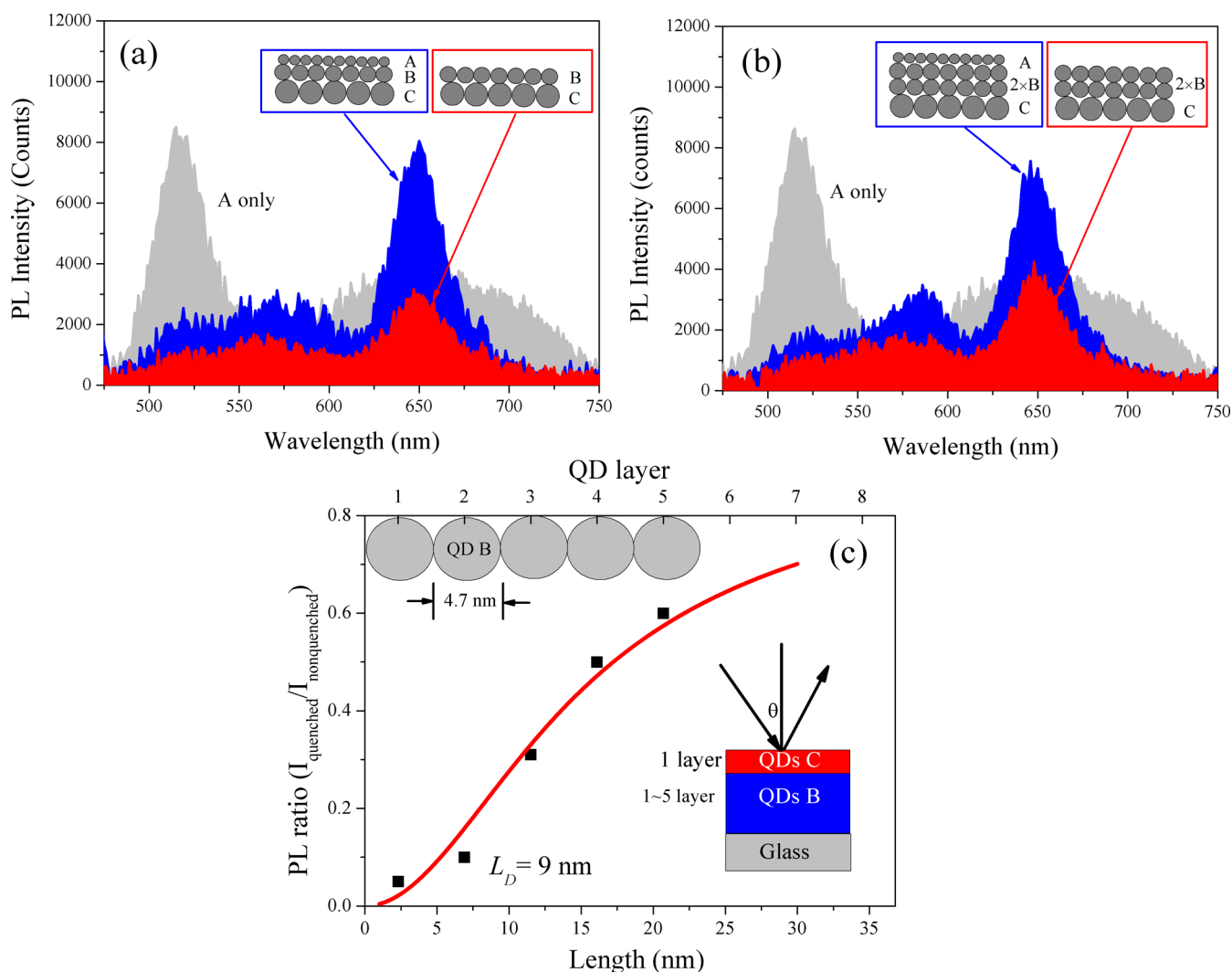
Figure 6. FRET in ordered QD films—PL analysis: (a) PL spectra of the ordered QD films A, B+C, and A+B+C. (b) PL spectra of the ordered QD films A, 2B+C, and A+2B+C. Excitation wavelength was 420 nm. (c) PL ratio between neat QD B film on glass and QD B film with top layer of QD C serving as quencher. The number of layers of QD B film varies from 1 to 5. The thicknesses of such films were estimated considering the mean size of individual QD together with capping agent (4.7 nm for QD B). Red line represents the theoretical fit using one-dimensional diffusion equation to extract exciton diffusion length L_D. The inset illustrates the structure of the measured samples.

conclude that the combination of realistic simulation of closely stacked QD layers, together with distributed-dipole FRET theory, can describe the process of energy transfer between QDs very well. Moreover, it is worth stressing that the FRET histograms have been calculated based on literature values and simulations; therefore, there is no free parameter in the presented theory.

When comparing experimental data and theoretical simulations in Figure 5, amplitudes of the theoretical curves had to be scaled down to reproduce the results. FRET lifetimes of 1−3 ns should, in comparison to the lifetime of an exciton in a QD (more than 20 ns in our case), lead to a FRET efficiency close to 100%. In reality, however, only about 50% of excitons are transferred, as one can deduce from the change in ratios of single-color spectra of the donor QDs (Figure 3). This originates from the contribution of several processes. First, agglomeration of QDs into clusters revealed by AFM images reduces the FRET efficiency. Second, the minor fast component in the intrinsic exciton dynamics, which has a lifetime of about 1 ns (Supporting Information), shows that there is an additional fast recombination competing with FRET.

This leads again to a decrease in the resulting FRET efficiency. Finally, the model assumes ideal intermixing of two sizes of QDs (Supporting Information). In the real films some islands of single-sized QDs might appear. Even if FRET between the QDs of the same size can take place, it does not contribute to the FRET presented in Figure 5 and diminish the resulting FRET amplitude.

Finally, the question may arise, why the previous reports of FRET on QDs could reproduce FRET rates well with a simple FRET theory applied to ideally stacked QD layers. This is likely a consequence of the fact that the two corrections introduced in this article have opposite effects. On one hand, the distribution of dipole moments increases the FRET rate between two close QDs. On the other hand, in randomly stacked layers the QD–QD distance is on average longer than that in the idealized cases.

Directed Energy Transfer between Layers of QDs with Different Sizes. In various devices it is of interest to maintain spatially directed energy transfer in QD films. For instance, in QD-sensitized solar cells, energy funneling toward QDs which are in contact with metal oxide enables charge separation even

for multiple layers of QDs. Such multilayer devices can absorb more light and provide significantly better performance. In order to investigate transport efficiency due to directed FRET between layers of QDs with different sizes, we have studied energy transfer in such a system.

We have prepared two types of ordered multilayer QD films, which are schematically depicted in Figure 6a,b. A monolayer of the C-type QDs (biggest QDs, lowest energy) was deposited as a bottom layer and covered by one or two monolayers of the B-type QDs (we get B+C, and 2B+C films, respectively). After measuring the PL of the films (B+C and 2B+C) as a reference, we deposit an additional monolayer of the A-type QDs on the top of the films (forming A+B+C and A+2B+C films) and determine changes in the PL after the deposition. Figure 6a,b illustrates the effect of the additional A-type layer on the PL spectra. The QD deposition was carried out by spin-coating and the formed "monolayers" are not ideal; nevertheless, they are very close to the actual monolayers (Supporting Information).

In the A+B+C film (see Figure 6a blue spectrum), the PL spectra exhibit a substantial increase in the C-type PL compared with the B+C film without the A-type layer (red spectrum). At the same time the emission from the A-type QDs is mostly quenched in the A+B+C sample (compare to the gray spectrum of the neat A-type film). Therefore, we can attribute the PL changes to the exciton transfer from A to C. We stress that the measurements were done under N_2 atmosphere, and low cw excitation (<0.5 mW/cm^2) and fast PL acquisition (30 s) were used. Therefore, we did not observe any indication of PL photoenhancement or photoquenching.

Now we will turn to the case where we deposit two monolayers of the B-type QDs (see Figure 6b). The PL intensity of C-type QDs in the 2B+C film (red spectrum) is more pronounced due to the energy transfer from QDs B. However, in the film A+2B+C (blue spectrum) the additional emission from QD A excitons is not as large as in the first case. This is expected since a large number of the excitons from the A-type QDs will not reach the C layer and will recombine within the B-type double-layer.

Quantitative analysis of the exciton flow can be performed by comparison of the integrated PL intensity within spectral regions corresponding to emission from different QDs. First of all, we can compare emission from the A-type QDs in the neat A-type film and in the ordered films. In both cases (A+B+C and A+2B+C films), we obtain that about 90% of all excitons is transferred away from the A-type QDs. This is expected due to relatively fast FRET (compared to the exciton lifetime).

Moreover, from the data we can obtain information about ratio of the excitons transferred from QDs A to QDs C (R_{AC}). In principle, the absolute R_{AC} value can be calculated; however, we need to use a number of assumptions and uncertain parameters introducing a significant error into the estimates. Alternatively, we can calculate the ratio between the R_{AC} value in the A+2B+C and A+B+C films (Supporting Information):

$$\frac{R_{A-C}^{A2BC}}{R_{A-C}^{ABC}} = \frac{I_C^{A2BC} - I_C^{2BC}}{I_C^{ABC} - I_C^{BC}} \qquad (6)$$

where I_C^{A2BC} denotes the PL intensity of the C-type QD in the AcL intensities). Experimentally we obtain the ratio 0.8, which means that the extra layer of the B-type QDs in the A+2B+C structure reduces the amount of the transferred excitons by 20%.

Since the additional B-type layer has a pronounced effect on the exciton funneling efficiency, it is of interest to quantify how the situation changes for an even higher number of deposited B-type monolayers. To quantify it, we have used an experiment commonly employed for the organic solar cell materials, where an emission from the thin film of conjugated polymers is measured first for the neat film and subsequently for the same film, where the surface is covered by an efficient PL quencher.[41,42] The ratio between PL from the neat and the quenched film is determined for several film thicknesses allowing to extract the so-called exciton diffusion length L_D, which determines an average distance that an exciton can travel in the material before its recombination.

In the ordered QD layers, the directed FRET can be evaluated analogously if we consider the energy acceptor (bigger QDs) as a "quencher". The experiment has been carried out for a sample consisting of only two sizes of QDs—the B-type QDs as a donor and the C-type QDs as an acceptor. In this case the analysis is simpler and allows us to quantify the transfer ratio. We formed a structure of B-type multilayers (1−5 layers), where the C-type QDs are deposited in the last step on the top of the B-type layers (see scheme in Figure 6c) (Supporting Information).

The exciton diffusion length can be extracted by monitoring changes in the PL from the B-type QDs for the increasing number of the B-type QD layers (i.e., layer thickness)—see Figure 6a. In particular, we calculated a ratio between PL intensity of the B-type QDs in the film B+C and the neat B film (the intensities were integrated over the whole emission band)—see Figure 6c (Supporting Information).

In case of the B-type monolayer, almost all (∼95%) excitons of the layer B were transferred to the layer C (see Figure 6c). At the same time we observe that the quenched B-type emission is accompanied by enhancement of the C-type PL (Supporting Information). This is an expected situation, since we have shown that the B−C FRET time is about 3 ns and a vast majority of the excitons with the mean lifetime of about 28 ns should be transferred. With increasing B-type layer thickness, many excitons do not reach the B/C interface and cannot be transferred to the C-type QD layer. This is leading to an increased B/C PL ratio.

We can obtain the exciton diffusion length $L_D = 9$ nm by using, analogously to the conjugated polymer films, a fitting model based on the one-dimensional exciton diffusion equation (red line in Figure 6c) (Supporting Information).[43] This shows that the excitation can only safely migrate via FRET through 1−2 monolayers of QDs, and for more layers, the funneling efficiency drops rapidly. It is worth stressing that this applies to a layer consisting of QDs with the same size.

We have developed in the previous sections a theoretical model describing FRET in random monolayers. Here we will demonstrate that the model can also be used for the ordered monolayers and reproduce our experimental results. The QD films for calculations were "prepared" by analogous consequent "deposition" of QDs of type C, B, and A, respectively, so that each size forms a random monolayer. The calculated structures can therefore simulate situations in the A+B+C and A+2B+C films, which were experimentally studied (see Figure 6b and c).

An example of the structure of three layers that we obtained is depicted in Figure 7 (left upper panel). In the calculated structure we pick a random QD of type A, where the exciton is created, and we find all neighboring QDs of type A, B, and C, which are less than 12 nm away. For each of them, we can
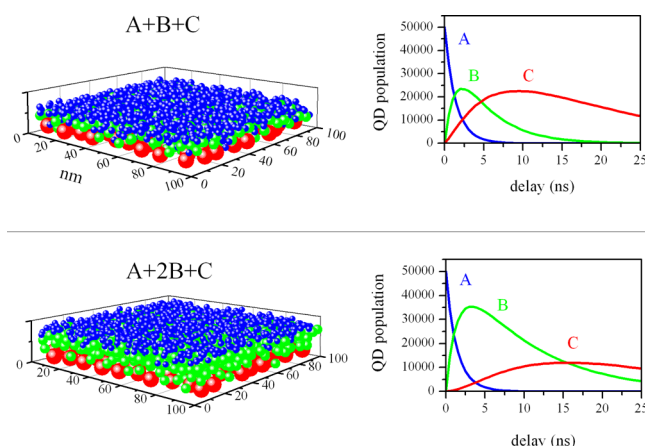
Figure 7. FRET in ordered QD films—Theoretical stimulation: Upper panel: Example of a QD film consisting of three subsequently deposited monolayers of A, B, and C QDs (blue, green, and red color, respectively). Calculated QD population after a random A-type QD is excited. Population is calculated for each size of QDs (A, blue line; B, green line; C, red line)—see text for details. Lower panel: Analogous film of QDs with a double layer of B-type QDs. Dynamics of QD population for the double-layer structure. The same color coding is used.

calculate FRET rate by using data in Table 1 and additional data for A−A and B−B transfer (Supporting Information).

Excitation in QD A can either recombine (for mean lifetime see Table 1) or can undergo FRET to another QD. The simulations use a Monte Carlo algorithm to choose which process takes place by a rate-weighted random choice between all possible transfer steps. The delay after excitation, when the process takes place, is calculated as $-\ln(r)/k_{\text{TOT}}$ (see SI for derivation of the expression), where k_{TOT} stands for total sum of rates of all incorporated processes and r stands for a random number from the uniform distribution (0, 1). After the process selection, the calculation is repeated until excitation has recombined.

By repeating the simulation 50 000× on films of three monolayers of QDs we consistently obtain that about 80% of all excitons initially created in QDs A are transferred to QDs C. Our calculations allow us also to plot the population of each type of QD after excitation (see Figure 6, upper right panel). It clearly demonstrates that the majority of excitons is transferred first to the B-type QDs and finally to the C-type QDs. On average the excitons on the way through the whole film travel about 14 nm (sum of center-to-center distances between QDs) before they reach the layer C, yet the losses are less than 20%. It takes about 10 ns to transport the vast majority of all excitons to layer C. We will now turn to the second experimentally investigated ordered film, where the two B-type layers are deposited (see Figure 7, lower left panel). Monte Carlo simulations show that the directed FRET becomes significantly slower due to the necessity to overcome the double layer of B, where the B−B transfer is relatively slow due to reduced spectral overlap of B-type absorption and emission. The resulting efficiency drops to 60%, i.e., the losses double due to the additional layer. At the same time, more than 15 ns is needed to transfer most of the excitons to the lowest QD layer.

We can now compare the experimental results with the calculations. First, the calculations can provide us with ratio of excitons transferred via FRET away from the QDs A. From the

calculations we obtain 94%, which is in good agreement with the experiment (about 90%).

Second, we can compare the ratio of the A to C exciton transfer for the two studied cases (A+B+C and A+2B+C). Theoretical calculations predict a drop of 25% (ratio 0.75). The experimental work gives us a very good agreement predicting a drop of 20% (ratio 0.8). The absolute ratios of the transferred excitons from A to C based on calculations (80% and 60% for the A+B+C case and A+2B+C case, respectively) can give us an idea of the obtainable efficiency. It is, however, likely that the calculations represent an idealized case, whereas the experimental value will be lower due to sample imperfections and possible carrier trapping.

CONCLUSIONS

We have presented a study of FRET in random densely packed QD layers by using TA spectroscopy on QDs with different sizes. We demonstrate a feasible way of fitting the TA spectra of QD layers with multiple sizes, which is able to separate FRET contribution from all intrinsic exciton decay pathways in QDs. The method is further capable of obtaining the whole FRET kinetics instead of a single lifetime.

We were able to reproduce the measured FRET dynamics by using theoretical calculations employing a realistic model of FRET in a random closely stacked QD layer. We clearly demonstrate that the distribution of dipole moments in QD is an important correction for the FRET in QD layers. This approach has provided a quantitative way to evaluate the energy migration process within QD systems.

Finally, we employ experiment and theory to determine energy funneling in ordered QD layers and calculate that energy funneling of 80% can be achieved through a three-layer system. We argue that QD-based optoelectronic devices with optimal design can highly benefit from efficient FRET.

ASSOCIATED CONTENT

Ⓢ Supporting Information
Sample preparation details, transient absorption spectra, calculation of FRET rate, distribution of QD−QD distance, morphology characterization of QD film, and directed energy transfer in ordered QD layers. This material is available free of charge via the Internet at http://pubs.acs.org.

AUTHOR INFORMATION

Corresponding Author
*E-mail: Tonu.Pullerits@chemphys.lu.se.
Author Contributions
Kaibo Zheng and Karel Žídek contributed equally to this work.
Notes
The authors declare no competing financial interest.

ACKNOWLEDGMENTS

REFERENCES

(1) Sambur, J. B.; Novet, T.; Parkinson, B. A. *Science* **2010**, *330*, 63−66.

(2) Kamat, P. *J. Phys. Chem. Lett.* **2013**, *4*, 908−918.

(3) Žídek, K.; Zheng, K.; Abdellah, M.; Lenngren, N.; Chábera, P.; Pullerits, T. *Nano Lett.* **2012**, *12*, 6393−9.

(4) Nozik, A. J.; Beard, M. C.; Luther, J. M.; Law, M.; Ellingson, R. J.; Johnon, J. C. *Chem. Rev.* **2010**, *110*, 6873−6890.

(5) Sargent, E. H. *Nat. Photonics* **2012**, *6*, 133−135.

(6) Ellingson, R. J.; Beard, M. C.; Johnson, J. C.; Yu, P.; Micic, O. I.; Nozik, A. J.; Shabaev, A.; Efros, A. L. *Nano Lett.* **2005**, *5*, 865−71.

(7) Karki, K. J.; Ma, F.; Zheng, K.; Žídek, K.; Mousa, A.; Abdellah, M.; Messing, M. E.; Wallenberg, L. R.; Yartsev, A.; Pullerits, T. *Sci. Rep.* **2013**, *3*, 2287.

(8) Abdellah, M.; Žídek, K.; Zheng, K.; Chábera, P.; Messing, M. E.; Pullerits, T. *J. Phys. Chem. Lett.* **2013**, *4*, 1760−1765.

(9) Milliron, D.; Hughes, S.; Cui, Y.; Manna, L. *Nature* **2004**, *430*, 190−195.

(10) Salter, C. L.; Stevenson, R. M.; Farrer, I.; Nicoll, C. A.; Ritchie, D. A.; Shields, A. J. *Nature* **2010**, *465*, 594−597.

(11) Kambhampati, P. *J. Phys. Chem. Lett.* **2012**, *3*, 1182−1190.

(12) Crooker, S.; Hollingsworth, J.; Tretiak, S.; Klimov, V. *Phys. Rev. Lett.* **2002**, *89*, 18−21.

(13) Hodes, G. *J. Phys. Chem. C* **2008**, *112*, 17778−17787.

(14) Santra, P. K.; Kamat, P. V. *J. Am. Chem. Soc.* **2013**, *135*, 877−85.

(15) Zheng, K.; Žídek, K.; Abdellah, M.; Torbjörnsson, M.; Chábera, P.; Shao, S.; Zhang, F.; Pullerits, T. *J. Phys. Chem. A* **2012**, *117*, 5919−5925.

(16) Choi, S.; Jin, H.; Bang, J.; Kim, S. *J. Phys. Chem. Lett.* **2012**, *3*, 3442−3447.

(17) Freiberg, A.; Godik, V.; Pullerits, T.; Timpmann, K. *Chem. Phys.* **1988**, *128*, 227−235.

(18) Grage, M.; Pullerits, T.; Ruseckas, A.; Theander, M.; Inganas, O.; Sundstrom, V. *Chem. Phys. Lett.* **2001**, *339*, 96−102.

(19) Franzl, T.; Koktysh, D. S.; Klar, T. A.; Rogach, A. L.; Feldmann, J.; Gaponik, N. *Appl. Phys. Lett.* **2004**, *84*, 2904−2906.

(20) Achermann, M.; Petruska, M. A.; Crooker, S. A.; Klimov, V. I. *J. Phys. Chem. B* **2003**, *107*, 13782−13787.

(21) Hosoki, K.; Tayagaki, T.; Yamamoto, S.; Matsuda, K.; Kanemitsu, Y. *Phys. Rev. Lett.* **2008**, *100*, 2−5.

(22) Kim, D. G.; Okahara, S.; Nakayama, M. *Phys. Rev. B* **2008**, *78*, 153301.

(23) Miyazaki, J.; Kinoshita, S. *Phys. Rev. B* **2012**, *86*, 035303.

(24) Lunz, M.; Bradley, A. L.; Gerard, V. A.; Byrne, S. J.; Gun'ko, Y. K.; Lesnyak, V.; Gaponik, N. *Phys. Rev. B* **2011**, *83*, 115423.

(25) Lee, J.; Govorov, A.; Kotov, N. *Nano Lett.* **2005**, *5*, 2063−2069.

(26) Chang, J. C. *J. Chem. Phys.* **1977**, *67*, 3901−3909.

(27) Madjet, M. E.; Abdurahman, A.; Renger, T. *J. Phys. Chem. B* **2006**, *110*, 17368−17281.

(28) Krueger, B. P.; Scholes, G. D.; Fleming, G. R. *J. Phys. Chem. B* **1998**, *102*, 5378−5386.

(29) Beenken, W. J. D.; Pullerits, T. *J. Chem. Phys.* **2004**, *120*, 2490−2495.

(30) Kagan, C.; Murray, C.; Nirmal, M.; Bawendi, B. G. *Phys. Rev. Lett.* **1996**, 1517−1520.

(31) Žídek, K.; Zheng, K.; Ponseca, C. S.; Messing, M. E.; Wallenberg, L. R.; Chábera, P.; Abdellah, M.; Sundström, V.; Pullerits, T.; Žídek, K. *J. Am. Chem. Soc.* **2012**, *134*, 12110−12117.

(32) Žídek, K.; Zheng, K.; Chábera, P.; Abdellah, M.; Pullerits, T. *Appl. Phys. Lett.* **2012**, *100*, 243111.

(33) Yu, W. W.; Qu, L.; Guo, W. *Chem. Mater.* **2003**, *15*, 2854−2860.

(34) Zheng, K.; Žídek, K.; Abdellah, M.; Chábera, P.; Abd El-sadek, M. S.; Pullerits, T. *Appl. Phys. Lett.* **2013**, *102*, 163119.

(35) Stokkum, I. H. M.; Larsen, D. S.; van Grondelle, R. *Biochim. Biophys.* **2004**, *1657*, 82−104.

(36) Schlegel, G.; Bohnenberger, J.; Potapova, I.; Mews, A. *Phys. Rev. Lett.* **2002**, *88*, 137401.

(37) Sharma, S. N.; Pillai, Z. S.; Kamat, P. V. *J. Phys. Chem. B* **2003**, *107*, 10088−10093.

(38) Brus, L. E. *J. Chem. Phys.* **1984**, *80*, 4403−4409.

(39) Wolcott, A.; Doyeux, V.; Nelson, C. A.; Gearba, R.; Lei, K. W.; Yager, K. G.; Dolocan, A. D.; Williams, K.; Nguyen, D.; Zhu, X. Y. *J. Phys. Chem. Lett.* **2011**, *2*, 795−800.

(40) Bruggeman, D. A. G. *Ann. Phys.* **1935**, *24*, 636−664.

(41) Menke, S. M.; Luhman, W. A.; Holmes, R. J. *Nat. Mater.* **2012**, *12*, 152−157.

(42) Mei, J.; Bradley, M. S.; Bulovic, V. *Phys. Rev. B* **2009**, *79*, 235205.

(43) Scully, S. R.; McGehee, M. D. *J. Appl. Phys.* **2006**, *100*, 034907.